Available online at www.sciencedirect.com
ScienceDirect
Journal of Sound and Vibration 317 (2008) 1017–1034
JOURNAL OF SOUND AND VIBRATION
www.elsevier.com/locate/jsvi

Vibration characteristics of floating slab track

Chen-Ming Kuo*, Cheng-Hao Huang, Yi-Yi Chen

Department of Civil Engineering, National Cheng Kung University, Taiwan, 1 University Rd., Tainan 70101, Taiwan

Received 23 August 2006; received in revised form 23 January 2008; accepted 29 March 2008
Handling Editor: L.G. Tham
Available online 15 May 2008

Abstract

Coupled equilibrium equations of suspended wheels and floating slab track system were solved with the fourth-order Runge–Kutta method to obtain the deflections, vibration velocities, and wheel–rail contact forces. The program was validated through several aspects. Cases with various vehicle speed, slab mass, and stiffness of slab bearing were analyzed to reveal the effects of slab bearing on track responses. The correlation between wheel–rail resonance and train speed was also discussed. It was found that rail deflections increase significantly as train speed increases. Although large slab mass may lower tuning frequency, it could also result in higher wheel–rail contact force and rail deflections. The floating slab track is effective in isolating loading above 10 Hz, which might present in some railway sections with irregularities. Adopting floating slab track for vibration control for environment along the railway may cause concerns about ride quality and track damages.

1. Introduction

The vibration induced by high-speed trains attracted attentions in Taiwan because the Taiwan high-speed railway (HSR) passes through the Tainan Science-based Industrial Park (TSIP), which is one of the major fab bases in Taiwan. Research projects were granted to resolve the vibration impacts on the hi-tech industrial park. Another vibration sensitive issue is about mass transit systems in urban areas. To mitigate vibration problems in tunnels of Xinzhuang–Luzhou line passing through vibration sensitive areas, Taipei Mass Rapid Transit System (Taipei MRTS) is introducing floating slab track (FST) in Taiwan for the first time. With these concerns, understanding vibration characteristics of slab track becomes a research topic.

FST, which basically consists of concrete slabs supported on resilient elements such as rubber bearings, has been used on modern rail transit system for years [1]. The design is aimed to reduce vibrations transmitting to the supporting foundations and surrounding areas. Floating slabs can be continuous if it is cast in-situ or discontinuous if it is constructed in discrete precast sections [2]. For discontinuous slabs, additional dynamic loads are induced at wheel–rail interface while a moving wheel on the track experiences a change of stiffness due to slab discontinuity. For heavy axle masses and high-speed trains, significant dynamic forces are induced at the wheel–rail interface.

*Corresponding author. Fax : +886 6 2358542.
E-mail address: ckuo@mail.ncku.edu.tw (C.-M. Kuo).

0022-460X/$ - see front matter © 2008 Elsevier Ltd. All rights reserved.
doi:10.1016/j.jsv.2008.03.051

In the USA, FST was pioneered at Washington, DC rapid transit system (WMATA) at 1970s. The WMATA floating slabs are continuous concrete slabs broken only by required construction joints spacing at 18.3 m. Later in 1980s, metro rapid system of Toronto and Hong Kong adopted floating track with short slabs of 1.45 m. Even shorter slabs were used in Hong Kong airport express and west railway in late 1990s. Although many document report its effectiveness, it remains controversial for underground railways due to interactions with the tunnel and surrounding soil [3]. Simple mass-spring models were often used to reveal isolation performance for the frequency above $\sqrt{2}$ times the natural frequency of the system. Jones [4] suggested that soft mats under the sleepers may be a useful countermeasure above 20 Hz and Nelson [5] models 9–12 dB reductions above 30 Hz.

Analysis of railway structure in early days is usually referred to Winkler's hypothesis in 1867, although the model is lack of shear transmission across adjacent springs, and the springs between rail and foundation are fully connected not being able to separate [6,7]. In 1946, Hetenyi presented analytical solutions for static loadings on an elastic beam supported by Winkler foundation [8]. Advanced dynamic models were developed by Frÿba [9] to reveal dynamic characteristics of train/track coupled systems. The models were improved by formulating track loadings with moving suspended masses and contact theory to research impact forces associated with structural parameters and moving speeds [10].

In order to design isolation systems tuned to the target frequency causing perceivable noise or vibrations, experiments were conducted with three small-scale isolator models and concluded that behavior of vibration isolation system is more complicated than predicted analytically [11]. Analytical model developed for FST could be found in the study of the rapid transit system of Singapore [12]. In the meantime, Crockeet and Pyke [13] evaluated vibration mitigation effects of FST on viaducts with the finite element package ANSYS. Recently, Hussein and Hunt [14] derive a three-dimensional model of a deep underground railway tunnel with FST based on Euler–Bernoulli beam theory. They further proposed a double-beam system and a complete treatment of the analysis for floating slab tracks [15]. In 2006, Lombaert et al. [16] developed a numerical model to investigate the reduction of free field vibrations by means of a floating slab track. They focused on the influence of dynamic track–soil interaction on the performance of the floating slab tracks and concluded that the insertion loss varies with stiffness of soil.

However, vibration of frequencies lower than the threshold might be amplified to some extend. Forrest and Hunt [17] found that vibration isolation effects of floating slab tracks could not be found at frequencies as low as predicted by simple theory. Any reductions are modest and there are some positions around the tunnel for which resilient slab bearings cause increased response at higher frequencies. Balendra et al. [18] also found that low-frequency vibration on FST is more significant than direct fastened track. In addition, some experiences showed that the maintenance costs are high and riding quality of trains is unsatisfied [19].

Although the aforementioned studies revealed the characteristics of the railway vibration from many aspects, in-depth discussions are still needed to clarify the effects of FST on track structure itself besides the general focus on environmental vibrations. The track responses were discussed comprehensively in this study.

2. Analytical equations of floating slab track

The wheel loading could be assumed as a pseudo-static force in simplified analyses [20]. For rigorous analyses, wheel–rail contact forces could be obtained by modeling bogie and carbody with mass-spring systems [21]. The carbody–bogie–track coupled systems require numerous parameters and complicated solving techniques. In this study, a moving vehicle consisting of springs connecting wheel and carbody was coupled with the track model via a contact spring. The equations are detailed as follows:

2.1. Rail

Rail was formulated with Euler beam theory which neglects shear deformations which were found relatively small in railway problems [22]. The accuracy of static or quasi-static analyses was found fairly good for a simply supported beam of finite length as long as the beam is long enough. The equilibrium equation of

rail is shown as

$$E_r I_r \frac{\partial^4 Z_r(x,t)}{\partial x^4} + m_r \frac{\partial^2 Z_r(x,t)}{\partial t^2} = -\sum_{i=1}^{N} F_{rsi}(t)\delta(x - x_i) + \sum_{j=1}^{4} P_j(t)\delta(x - x_{pj}) \tag{1}$$

where Z_r is the vertical deflection of rail, E_r the Young modulus of rail, I_r the moment of inertia of rail, m_r the rail mass of unit length, F_{rsi} the fastening force, P_j the wheel–rail force, N the amount of rail clips

x_{p1}: the distance between the rear wheel and the origin $= x_{p0} + vt$
x_{p2}: the distance between the second rear wheel and the origin $= x_{p0} + h_w + vt$
x_{p3}: the distance between the second wheel and the origin $= x_{p0} + (h_w + h_c) + vt$
x_{p4}: the distance between the rear wheel and the origin $= x_{p0} + (2h_w + h_c) + vt$
v: train speed
h_w: spacing of the axles in a bogie
h_c: spacing between the inner axles of the bogies of the same vehicle

According to Ritz method, a shape function, shown as Eq. (2), was substituted into Eq. (1) to elaborate variable separation into Eq. (3). By solving Eq. (3), mode shapes and associated amplitudes of rail vibration can be obtained. The deflections of rail are then calculated with superposition of mnr terms of modes.

$$Z_r(x,t) = \sum_{k=1}^{\text{mnr}} \phi_k(x) q_k(t) \tag{2}$$

where $\phi_k(x) = \sin k\pi x/l$, mnr is the number of modes, l the length of the modeled rail

$$\ddot{q}_k(t) + \frac{E_r I_r}{m_r}\left(\frac{k\pi}{l}\right)^4 q_k(t) = -\frac{2}{m_r l_r}\sum_{i=1}^{N} F_{rsi}(t)\phi_k(x_{si}) + \frac{2}{m_r l_r}\sum_{j=1}^{4} P_j(t)\phi_k(x_{pj}) \tag{3}$$

2.2. Floating slabs

The floating slabs were also formulated with Euler beams as shown in Fig. 1. The slabs are discretely loaded with rail seat forces and reactions of slab bearings. The equilibrium equation is shown as follows:

$$E_s I_s \frac{\partial^4 Z_s(x,t)}{\partial x^4} + \frac{M_s}{l_s}\frac{\partial^2 Z_s(x,t)}{\partial t^2} = \sum_{i=1}^{N} F_{rsi}(t)\delta(x - x_{si}) - \sum_{i=1}^{NP} F_{sfi}(t)\delta(x - x_{fi}) \tag{4}$$

where F_{rsi} is the jth rail seat force $= C_p[\dot{Z}_r(x_{si},t) - \dot{Z}_s(x_{si},t)] + K_p[Z_r(x_{si},t) - Z_s(x_{si},t)]$, F_{sfi} is the jth slab supporting force $= C_b\dot{Z}_s(x_{fi},t) + K_b Z_s(x_{fi},t)$, C_p the damping coefficient of rail clips, K_p the spring coefficient of rail clips, C_b the damping coefficient of slab bearings, K_b the damping coefficient of slab bearings, x_{si} the position of the ith rail seat; x_{fi} the position of the ith slab bearing.

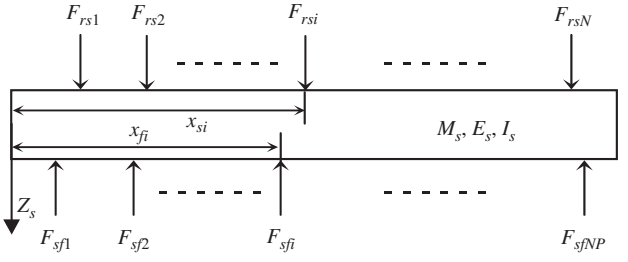

Fig. 1. Slab model.

Vertical deflections of slabs, $Z_s(x,t)$, were assumed as Eq. (5) which accounts slab deformation characteristics and further variable separation [23]

$$Z_s(x,t) = \sum_{m=1}^{mns} X_m(x) A_m(t) \tag{5}$$

where $X_1 = 1$, $X_2 = \sqrt{3}(1 - 2x/l_s)$ $X_m = \mathrm{Cosh}(\varepsilon_m x) + \mathrm{Cos}(\varepsilon_m x) - C_m[\mathrm{Sinh}(\varepsilon_m x) + \mathrm{Sin}(\varepsilon_m x)]$, $m \geqslant 3$, C_m, ε_m the parameters in expression for X_m, shown in Table 1.

By substituting Eq. (5) into Eq. (4), the equilibrium equation of floating slab, becomes the form as shown below:

$$\ddot{A}_m(t) + \frac{E_s I_s l_s \varepsilon_m^4}{M_s} A_m(t) = \sum_{i=1}^{NP} \frac{F_{rsi}(t)}{M_s} X_n(x_{si}) - \sum_{i=1}^{NP} \frac{F_{sfi}(t)}{M_s} X_n(x_{fi}) \tag{6}$$

2.3. Vehicle model

Since comprehensive vehicle models consisting of tens of degrees of freedom are out of the scope of this study, a simple 1/8 car model shown in Fig. 2 was adopted. The equilibrium equations include two parts, the sprung carbody and the unsprung wheel.

Sprung carbody:

$$M_{vs}\ddot{Z}_{vj}(t) + C_v\left[\dot{Z}_{vj}(t) - \dot{Z}_{wj}(t)\right] + K_v\left[Z_{vj}(t) - Z_{wj}(t)\right] = M_{vs}g \tag{7}$$

Unsprung wheel:

$$M_{vu}\ddot{Z}_{wj}(t) - C_v[\dot{Z}_{vj}(t) - \dot{Z}_{wj}(t)] - K_v[Z_{vj}(t) - Z_{wj}(t)] = M_{vu}g - P_j(t) \tag{8}$$

where Z_{vj} is the vertical deflection of the jth carbody, M_{vs} the mass of a carbody, Z_{wj} the vertical deflection of the jth wheel, M_{vu} the mass of an wheel, C_v the damping coefficient of suspension, K_v the spring coefficient

Table 1
Values of C_m and ε_m

m	1	2	3	4	5	6
C_m	–	–	0.982502	1.000777	0.999966	1.000000
$\varepsilon_m l_s$	0	0	4.73004	7.85320	10.99560	$(2m-3)\pi/2$

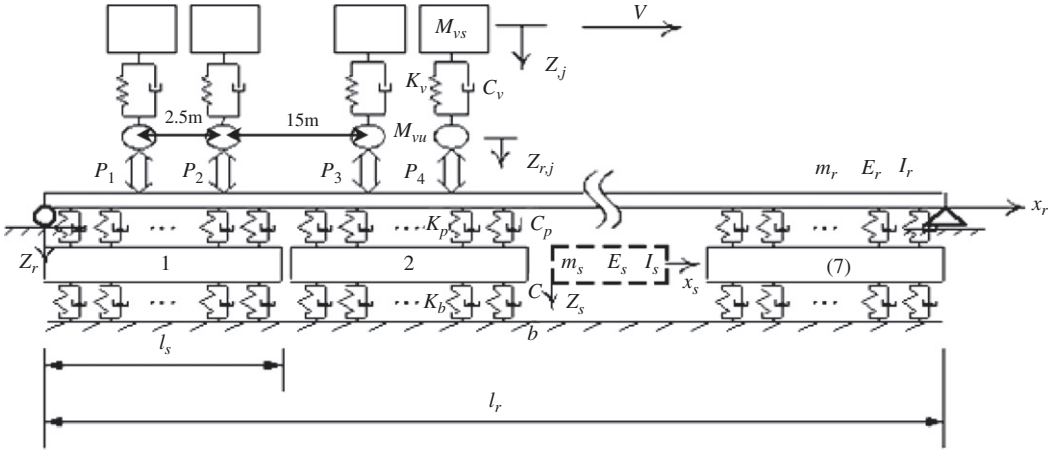

Fig. 2. Model of simplified vehicle on floating slab track.

of suspension

$$P_j(t) = \begin{cases} K_c[Z_{wj}(t) - Z_r(x_{pj}, t)] & \text{if} \quad Z_{wj}(t) - Z_r(x_{pj}, t) > 0 \\ 0 & \text{if} \quad Z_{wj}(t) - Z_r(x_{pj}, t) \leqslant 0 \end{cases}$$

K_c the coefficient of contact spring ($= 810^{10}$ N/m).

Finally, all the variable separated equations are coupled and rearrangement as shown below:

$$\ddot{\mathbf{q}} + \frac{E_r I_r}{m_r}\left(\frac{k\pi}{l}\right)^4 + \frac{2}{m_r l_r}\left\{\begin{array}{l} C_p \sum_{i=1}^{N}\left[\dot{\mathbf{q}}^{\mathrm{T}}\phi(x_{s_i})\phi(x_{s_i}) - \dot{\mathbf{A}}^{\mathrm{T}}\mathbf{X}(x_{s_i})\phi(x_{s_i})\right] \\ +K_p \sum_{i=1}^{N}\left[\mathbf{q}^{\mathrm{T}}\phi(x_{s_i})\phi(x_{s_i}) - \mathbf{A}^{\mathrm{T}}\mathbf{X}(x_{s_i})\phi(x_{s_i})\right] \end{array}\right\} + \frac{2}{m_r l_r} K_c \sum_{j=1}^{4}\left[\mathbf{q}^{\mathrm{T}}\phi(x_{p_j})\phi(x_{p_j}) - Z_{w_j}\phi(x_{p_j})\right] = 0 \tag{9}$$

$$\ddot{\mathbf{A}} + \frac{E_s I_s l_s \varepsilon_m^4}{M_s}\mathbf{A} + \frac{1}{M_s}\left\{\begin{array}{l} C_p \sum_{j=1}^{NP}\left[\dot{\mathbf{A}}^{\mathrm{T}}\mathbf{X}(x_{s_j})\mathbf{X}(x_{s_j}) - \dot{\mathbf{q}}^{\mathrm{T}}\phi(x_{s_j})\mathbf{X}(x_{s_j})\right] \\ +K_p \sum_{j=1}^{NP}\left[\mathbf{A}^{\mathrm{T}}\mathbf{X}(x_{s_j})\mathbf{X}(x_{s_j}) - \mathbf{q}^{\mathrm{T}}\phi(x_{s_j})\mathbf{X}(x_{s_j})\right] \end{array}\right\} + \frac{1}{M_s}\left\{K_b \sum_{j=1}^{NP}\mathbf{A}^{\mathrm{T}}\mathbf{X}(x_{s_j})\mathbf{X}(x_{s_j}) + C_b \sum_{j=1}^{NP}\dot{\mathbf{A}}^{\mathrm{T}}\mathbf{X}(x_{s_j})\mathbf{X}(x_{s_j})\right\} = 0 \tag{10}$$

$$\ddot{\mathbf{Z}}_{vj} + \frac{C_v}{M_{vs}}\dot{\mathbf{Z}}_{vj} - \frac{C_v}{M_{vs}}\dot{\mathbf{Z}}_{wj} + \frac{K_v}{M_{vs}}\mathbf{Z}_{vj} - \frac{K_v}{M_{vs}}\mathbf{Z}_{wj} = g \tag{11}$$

$$\ddot{\mathbf{Z}}_{wj} - \frac{C_v}{M_{vu}}\dot{\mathbf{Z}}_{vj} + \frac{C_v}{M_{vu}}\dot{\mathbf{Z}}_{wj} - \frac{K_c}{M_{vu}}\mathbf{q}^{\mathrm{T}}\phi(x_{p_j}) - \frac{K_v}{M_{vu}}\mathbf{Z}_{vj} + \frac{K_v + K_c}{M_{vu}}\mathbf{Z}_{wj} = g \tag{12}$$

3. Model validation

Runge–Kutta method was adopted to solve the aforementioned equations. A suspended mass moving along a simply supported beam, shown as Fig. 3 and Table 2, was analyzed. The results were compared with the theoretical solutions [24]. Fig. 4(a) shows the time histories of midpoint deflection obtained via the program developed in this study, whereas Fig. 4(b) illustrates results from the analytical solution, finite element analysis by Yang et al. The time histories of vibration acceleration calculated with the program were shown in Fig. 5(a), and those of Yang's study were shown in Fig. 5(b). Either from rail deflection or vibration acceleration point of view, the curves with different approaches match very well for both single mode approximation and multimode superposition.

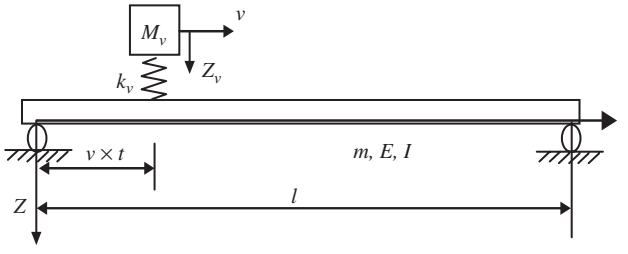

Fig. 3. Validation model (a suspended mass moving on a simply supported beam).

Table 2
Parameters of the validation model

M_v (suspended mass)	5750 kg
k_v (suspension stiffness)	1.595×10^6 N/m
v (moving speed)	27.78 m/s
l (length of beam)	25 m
E (beam's elastic modulus)	2.87×10^9 N/m^2
I (beam's inertia of momentum)	2.9 m^4
m (beam mass of a unit length)	2303 kg/m

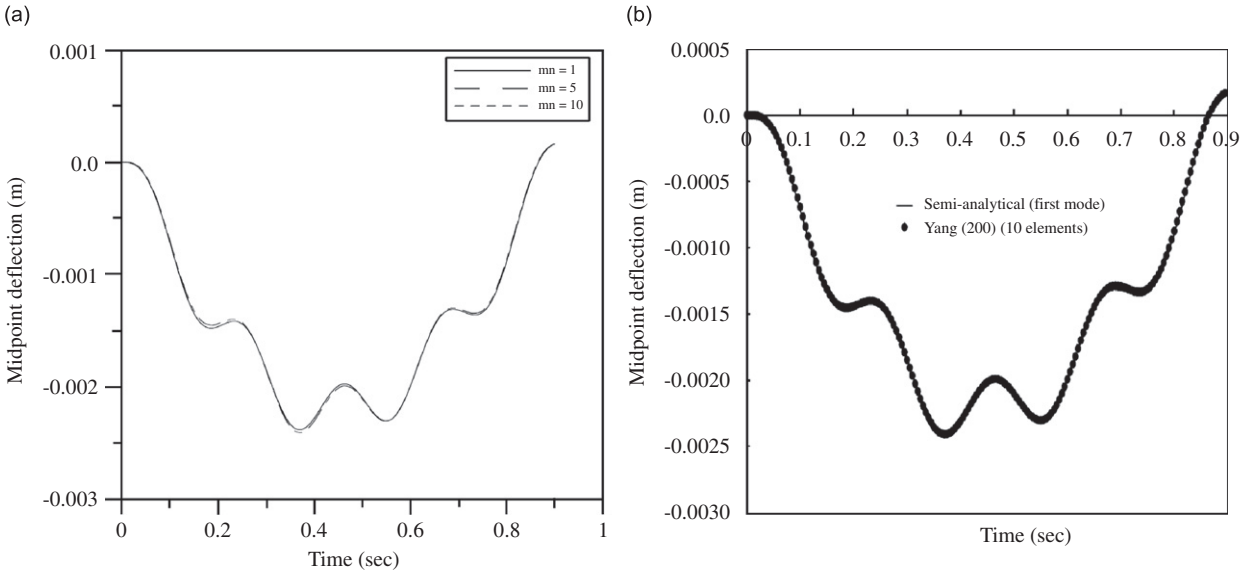

Fig. 4. Midpoint deflection of simply supported beam under moving mass. (a) Present result (model superposition method) and (b) Yang et al.

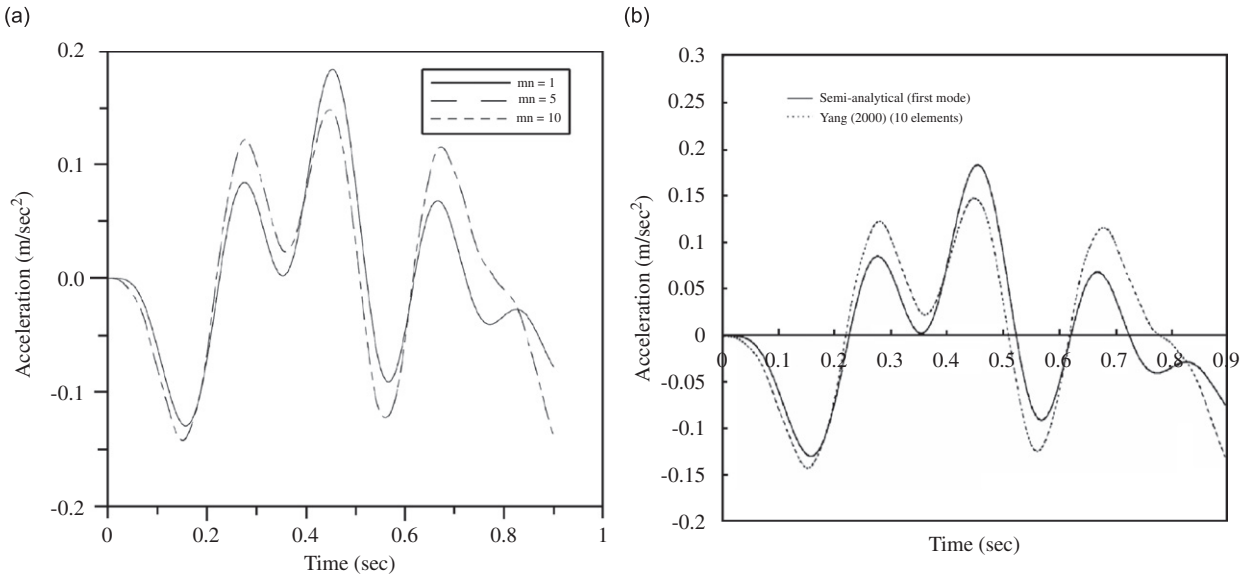

Fig. 5. Acceleration of moving sprung mass. (a) Present result (model superposition method) and (b) Yang et al.

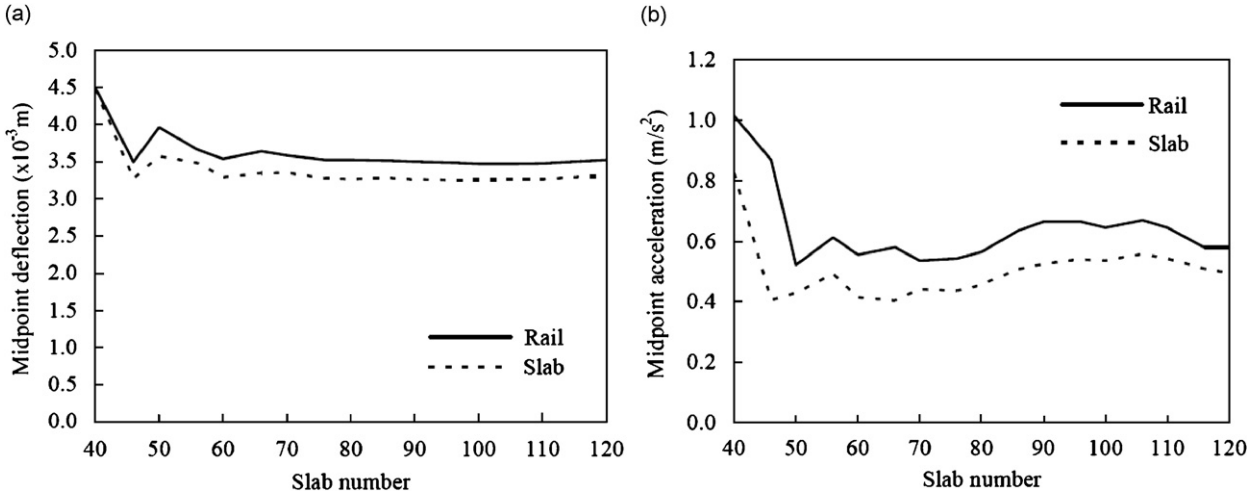

Fig. 6. Convergence of midpoint responses with various length of track model.

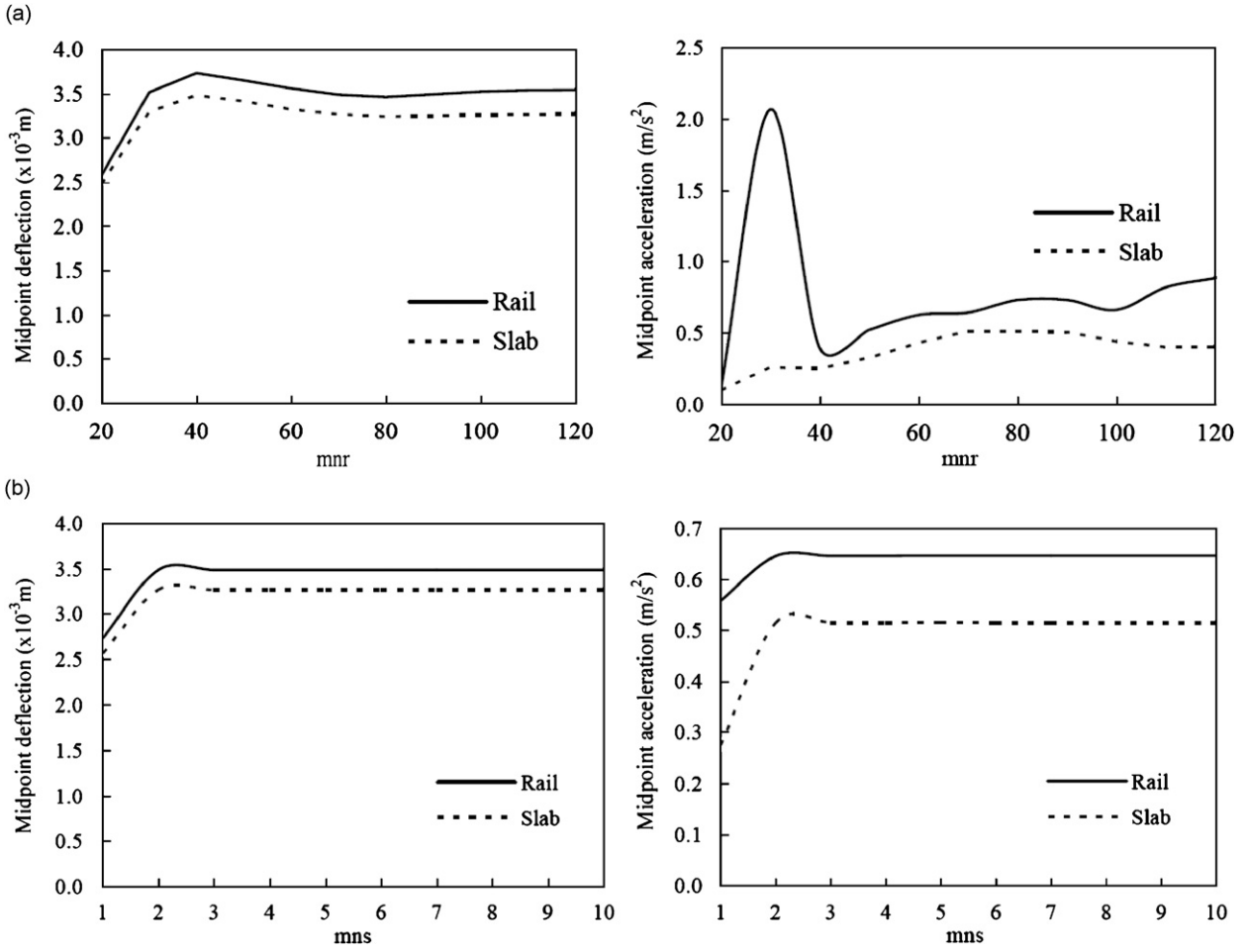

Fig. 7. Convergence of midpoint responses with (a) numbers of rail modes and (b) numbers of slab modes.

The length of track model is important to solving efficiency and accuracy. Fig. 6 shows midpoint responses calculated with various model lengths under moving load of 22 m/s. It reveals that responses of rail and slab may converge as model length or number of modes increases, although acceleration does not converge as smooth as deflection does. It is believed that a better convergence of vibration accelerations can be achieved if time step in dynamic analysis can be further reduced for higher output resolution. The extent of 80 slabs, 104 m, was determined to be the model length in this study to minimize the cut-off error.

Since the deflections of rail and slabs were calculated with modal superposition, the numbers of modes are also crucial to computation accuracy and efficiency. Fig. 7 shows the convergence of midpoint deflection and acceleration of rail with various numbers of rail modes. It is clear that the convergence of vibration acceleration dominates the number of modes. Seventy modes for rail and three modes for slab were used in the following analyses to ensure computation efficiency and accuracy.

In order to justify effectiveness of vibration mitigation for the environment, analysis results were compared with two track models having different slab bearing stiffness, "with vibration isolation" (5.8 MN/m) and "without vibration isolation" (580 MN/m). Fig. 8 illustrates that FST is effective in reducing forces by about 33% from transmitting to subgrade. In order to reveal the reduction mechanism, the frequency spectrums of rail clip forces were compared as shown in Fig. 9. Fig. 9(a) illustrates that the rail clip force on a smooth railway section is basically a low-frequency force. The system with slab bearings reduces rail clip forces beyond 19 Hz, which is $\sqrt{2}$ times the fifth characteristic frequency of the system according to Table 5. Fig. 9(b) further found that the spectrum also conforms to theoretical transmissibility and the perception that very low-frequency vibration cannot be effectively controlled. In addition, the amplitudes of loading frequencies beyond 10 Hz were found fractional compared to those of low frequencies due to lack of track irregularities in the analysis. Hence, the vibration isolation only plays a minor role in reduction of force transmission. Force redistribution among slab bearings are believed to be the major cause of reduction of force transmission in smooth railway sections. Detailed discussion on this issue and the influence of track roughness will be covered in the upcoming research.

Fig. 10 shows time history of force of the rail clip at the midpoint of the model. The maximum uplifting force is about 1 kN, which is less than normal strength of rail clips (8–20 kN). Maintenance of rail clips may not be a critical issue in floating slab tracks.

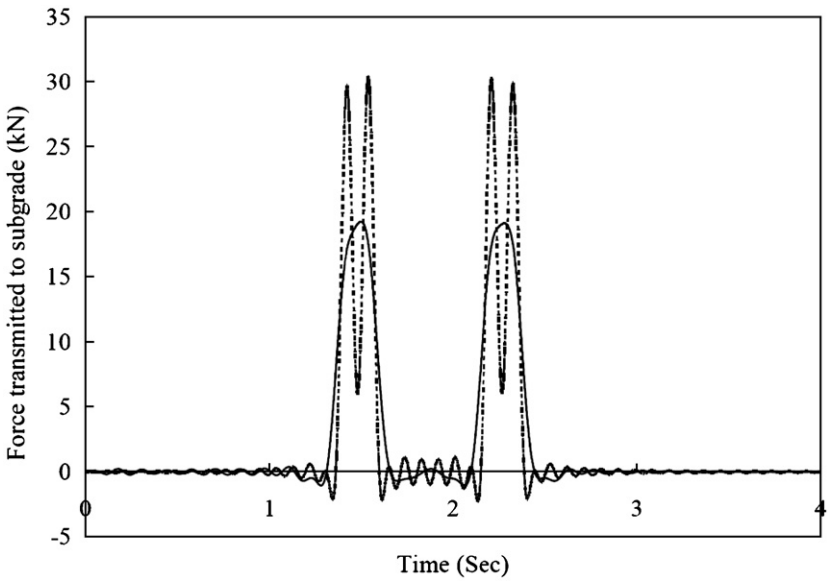

Fig. 8. Time history of force transmitted to subgrade at the midpoint for tracks: (—) with vibration isolation, and (- - -) without vibration isolation at train speed = 22 m/s.

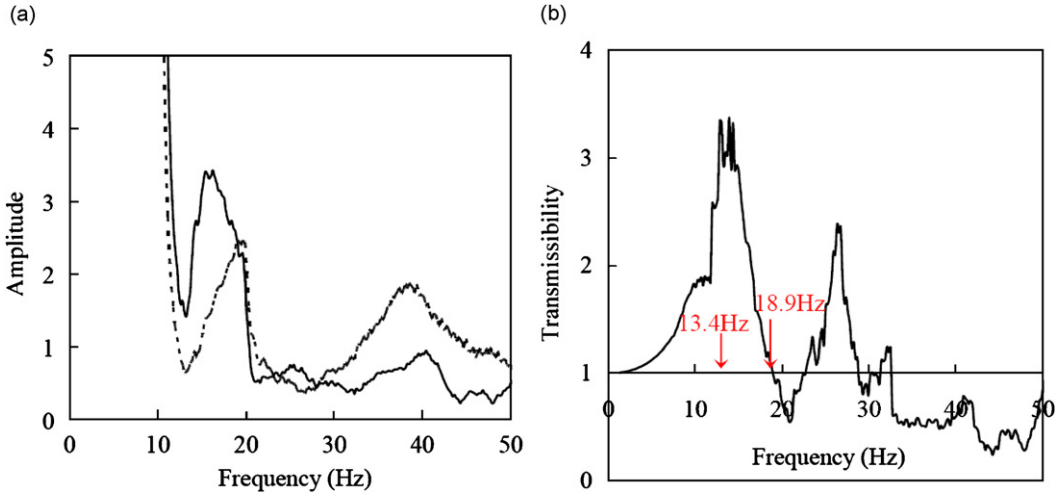

Fig. 9. Reduction of rail clip force: (a) comparison of frequency spectrum of rail clip forces, (—) with vibration isolation, (- - -) without vibration isolation at train speed = 22 m/s; and (b) transmissibility of the system with vibration isolation.

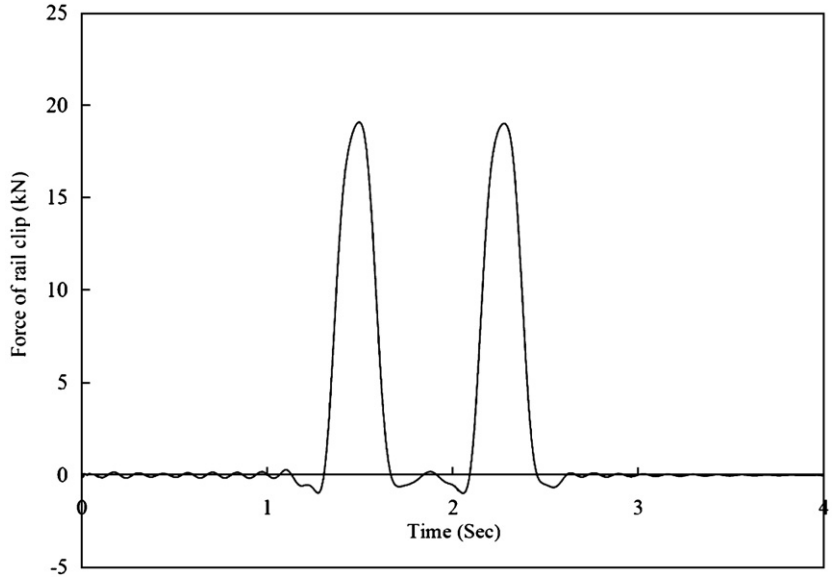

Fig. 10. Time history of force experienced by the rail clip at the midpoint for train speed = 22 m/s.

4. Responses of floating slab track

Analyses were conducted with the model introduced above to examine the rail deflection, wheel–rail contact force, velocity and acceleration of slabs for different designs of floating slab track. All the analyses were done without any wheel or rail surface irregularities. The loading configuration and track parameters are shown in Tables 3 and 4. The midpoint deflections shown in Fig. 11 illustrate two peaks reflecting passages of front bogie and rear bogie. The axles in the same bogie are too close to be distinguished with the analysis time step and number of modes. The maximum deflection is about 3.5 mm, which is reasonable as compared with the measured data, 3–5 mm, in Hong Kong FST system. The maximum deflection of rail under 70 m/s moving loads was predicted to be 4.7 mm with the model.

Fig. 12 shows the time histories of wheel–rail contact forces. In order to explain the curve distortion in the figure, analyses of initially zero deflection and initially static loaded were conducted. Both results still showed

Table 3
Parameters of the analyzed floating slab track

Mass of rail (m_r)	60.34 kg/m
Young's modulus of rail (E_r)	2.0×10^{11} N/m^2
Moment of inertia of rail (I_r)	3.05×10^{-5} m^4
Rail clip spacing (H_p)	0.65 m
Stiffness of rail clip (K_p)	100 MN/m
Damping of rail clip (C_p)	30000 N s/m
Mass of slab (M_s)	1640 kg
Young's modulus of slab (E_s)	3.5×10^{10} N/m^2
Moment of inertia of slab (I_s)	1.89×10^{-3} m^4
Slab length (l_s)	1.25 m
Spacing of slab bearing (H_b)	0.65 m
Stiffness of slab bearing (K_b)	5.8 MN/m
Damping of slab bearing (C_b)	35000 N s/m

Table 4
Parameters of train wheel used in the analysis

Mass of carbody (W_{car})	41750 kg
Stiffness (2nd suspension) (K_2)	2.65×10^5 N/m
Damping (2nd suspension) (C_2)	4.51×10^4N s/m
Mass of bogie frame (M_b)	3040 kg
Stiffness (prim. suspend.) (K_1)	1.18×10^6 N/m
Damping (prim. suspend.) (C_1)	3.92×10^4 N s/m
Mass of wheel (m_w)	890 kg

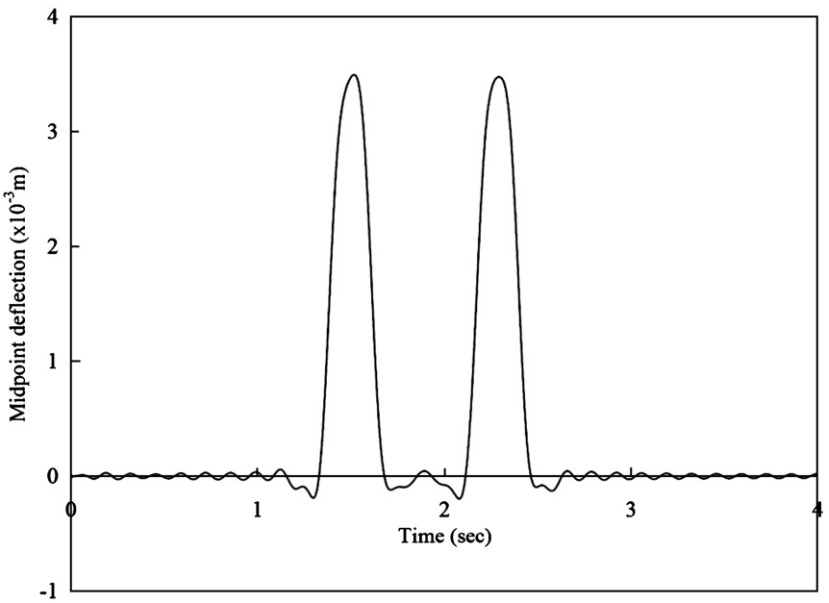

Fig. 11. Time history of rail deflection at midpoint of the model for train speed = 22 m/s.

distortion in the beginning. Hence, the transient states of track deflections upon starting moving might be responsible to the disturbance of time history curves in the beginning part. The middle part of the curves is reasonably steady since the track model is smooth without irregularity. Whereas the right-hand side of the curves showing minor distortion could be attributed to the boundary constraints.

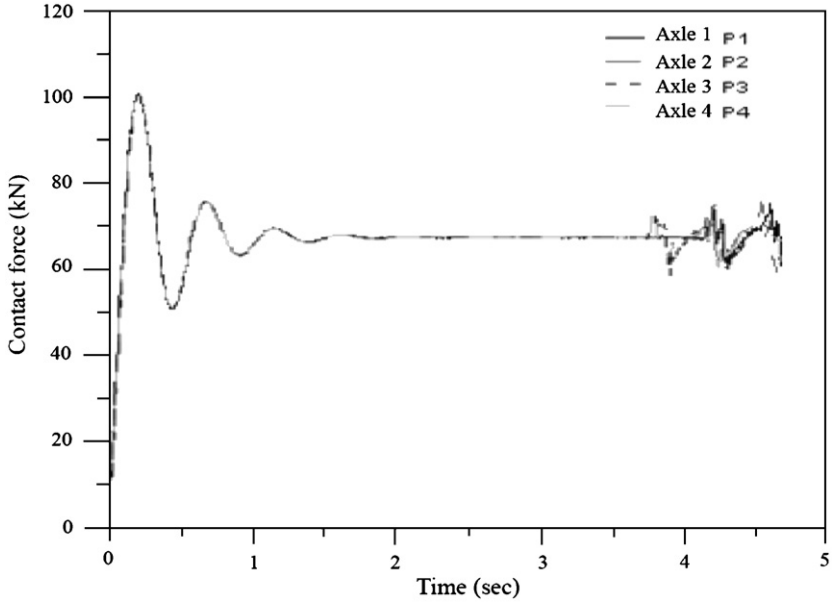

Fig. 12. Time history of wheel–rail contact force at train speed = 22 m/s.

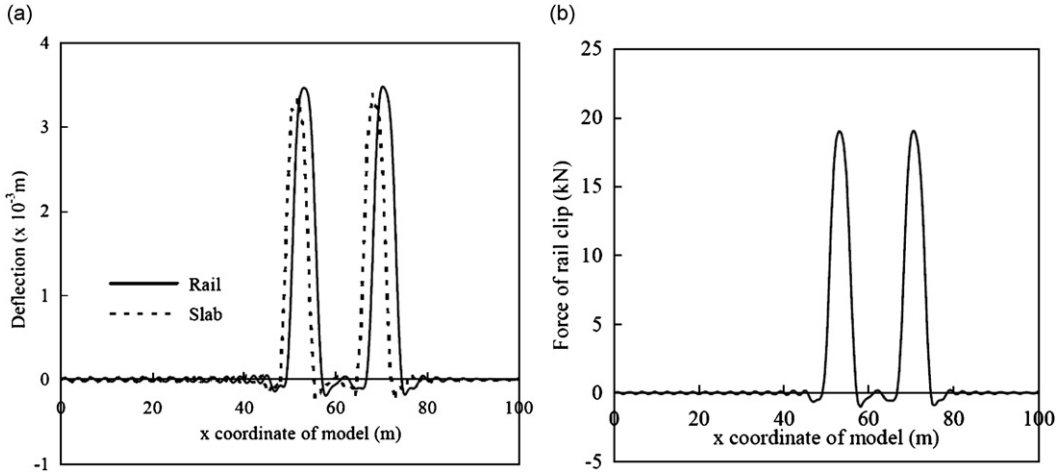

Fig. 13. Deflection of rail and slabs and force of rail clip along the track model at $t = 2.338$ s for the case of train moving at 22 m/s.

Although the short slab acts like rigid body motions in the vertical direction, differential deflections do exist between slabs. The force of rail clip depends on differential deflection between slab and rail. Fig. 13(a) illustrates the deflection of rail and slabs at $t = 2.338$ s and Fig. 13(b) shows the forces of rail clips. The maximum downward pressure is about 19 kN and the maximum uplifting force is about 1 kN, which is far less than uplifting capacity of rail clips (8–20kN). Deterioration of rail clips might not be a critical concern for floating slab tracks.

4.1. The effect of rail clip on rail vibration

In order to evaluate the consequences of various rail clips, three levels of rail clip stiffness were considered. 25 MN/m represents the normal stiffness in the field. Stiff rail clip, 100 and 200 MN/m, were assumed for the cases of deflection control design and aged pads. The resonant frequencies of the track system were estimated as following steps to interpret rail vibration at different loading speed.

Vibration frequency of Euler beam with clamped ends [25] $f_n = 22.4/2\pi\sqrt{EI/\rho l^4}$

Equivalent length for a continuously supported Euler beam $l = 2\pi\sqrt[4]{4EI/u}$

Substituting equivalent length into frequency equation to have $f_n = 0.04515\sqrt{u/\rho}$.

The modulus of elasticity of the track support, u, is a lumped parameter combining stiffness under the rail. It was estimated by calculating stiffness of rail clip and slab bearing in series. Table 5 shows that the major characteristic frequencies of systems with different supporting stiffness are all below 10 Hz. The data agrees with the conclusion made by Mair [26] that the resonant frequency of the track itself is not significantly dependent on the variable support stiffness. Also, the major resonant frequencies match the results proposed by Takemiya [27]. Takemiya also found that rail clip spacing was less critical in track resonance. As shown in Table 6, rail clip spacing corresponds to relatively high frequencies of periodical loading patterns.

The impact factor of rail deflection and increase rate of contact force, shown as Eqs. (13) and (14), were compared to reveal the dynamic effects with respect to static responses. It was found that rail deflection, Fig. 14(a) and contact force, Fig. 14(b) both increase with vehicle speed regardless of rail clip stiffness. Since high vehicle speed causes high loading frequency as shown in Table 6, the speeds around 55 and 75 m/s producing the fundamental track resonant frequencies cause amplifications. This implies that the dynamic impact on rail should be treated carefully on FST lines for specific speeds above 50 m/s (180 kph). Noticing that soft rail clip is significantly effective in alleviating wheel–rail contact force even at high speed, as shown in Fig. 14(b).

Table 5
Characteristic frequencies of rail

K_p (MN/m)	25	100	200	25	25
K_b (MN/m)	5.8	5.8	5.8	4.4	2.9
u (MN/m^2)	7.28	8.45	8.68	5.78	4.01
1st mode (Hz)	3	3	3	2	2
2nd mode (Hz)	5	6	6	5	4
3rd mode (Hz)	8	8	8	7	6
4th mode (Hz)	10	11	11	9	8
5th mode (Hz)	13	14	14	11	10

Table 6
Loading frequencies at various moving speeds

Speed (m/s)	Periodical loading sources			
	Axle spacing		Slab bearing spacing	Clip spacing
	15 m	2.5 m	1.25 m	0.65 m
20	1.3	8	16	31
25	1.7	10	20	39
30	2.0	12	24	46
35	2.3	14	28	54
40	2.7	16	32	62
45	3.0	18	36	69
50	3.3	20	40	77
55	3.7	22	44	85
60	4.0	24	48	92
65	4.3	26	52	100
70	4.7	28	56	108
75	5.0	30	60	115
80	5.3	32	64	123

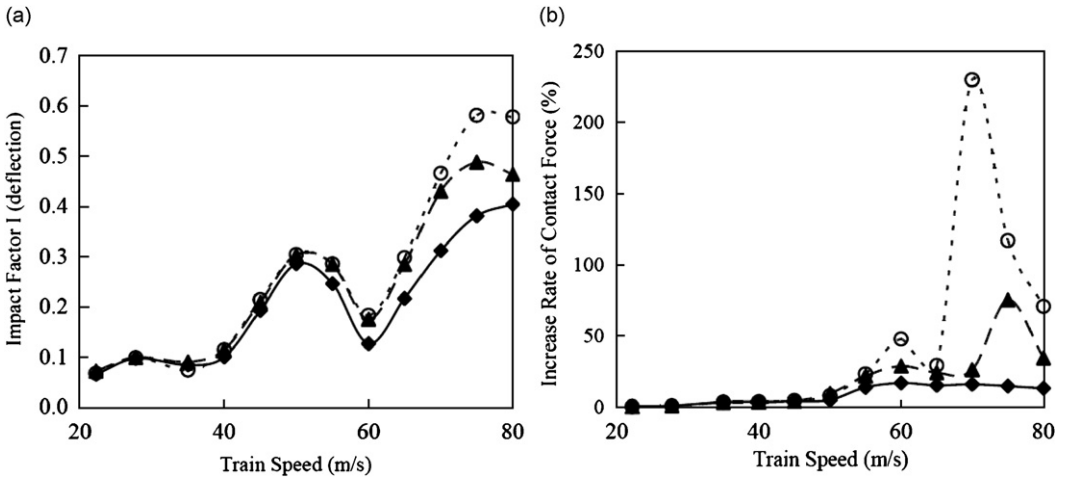

Fig. 14. Comparisons of (a) impact factor of maximum rail deflection and (b) increase rate of wheel–rail contact force of the tracks with rail clip stiffness, 25 kN/mm (♦), 100 kN/mm (▲), and 200 kN/mm (○) at various train speeds.

Impact factor (of rail deflection):

$$I = \frac{(Z_r)_{\mathrm{dyn}} - (Z_r)_{\mathrm{sta}}}{(Z_r)_{\mathrm{sta}}} \tag{13}$$

Increase rate (of contact force):

$$\frac{\max P_{\mathrm{dyn}}(t) - \max P_{\mathrm{sta}}(t)}{\max P_{\mathrm{sta}}(t)} \times 100\% \tag{14}$$

where $(Z_r)_{\mathrm{dyn}}$ is the maximum rail deflection of dynamic analysis, $(Z_r)_{\mathrm{sta}}$ the maximum rail deflection of static analysis, $\max P_{\mathrm{dyn}}(t)$ the maximum contact force of dynamic analysis, $\max P_{\mathrm{sta}}(t)$ the maximum contact force of static analysis.

4.2. The effect of slab bearing on rail vibration

In contrary to rail clip which is sensitive in wheel–rail force but insignificant in track deflection, slab bearing stiffness significantly affects track deflection as shown in Fig. 15(a). In Fig. 15(b), wheel–rail contact force of the system with soft slab bearing was found larger than stiff bearings at 60 m/s. This result contradicts the expectation of soft slab bearings for vibration mitigation. Essentially, the general goal of vibration control is to reduce vibration transmission to subgrade, not to reduce the vibration in rail or the vehicle. Hsu et al. [28] proposed a similar viewpoint that vibration propagation might be confined to result in enlarging responses on rail and vehicles. The trade-off between environmental vibration concerns and train comfort/safety should always be considered by the track engineers.

The computed responses were further transformed into frequency spectrum, as shown in Fig. 16. The spectrum shows that slab bearing stiffness dominates the vibration characteristics of rail in low-frequency range, whereas moving speed is the major factor in the frequency range above 30 Hz. The figure also implies that vehicles moving on floating slab track, which has soft slab bearings, might encounter more swaying or bouncing due to higher vibration in low-frequency range. The peaks in the curves also justified the data in Table 6.

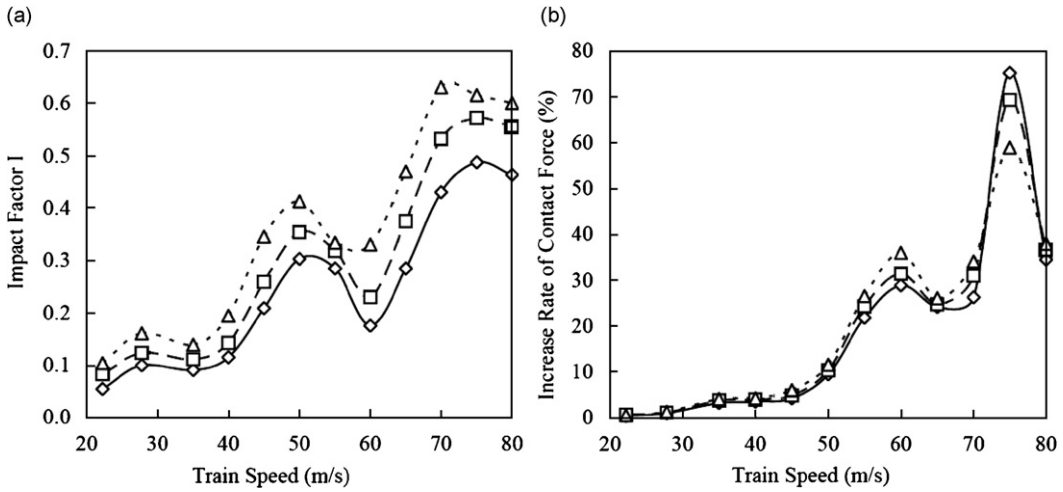

Fig. 15. Comparisons of (a) impact factor of maximum rail deflection and (b) increase rate of wheel–rail contact force of the tracks with slab bearing stiffness, 5.8 kN/mm (◇), 4.4 kN/mm (□), and 2.9 kN/mm (△) at various train speeds.

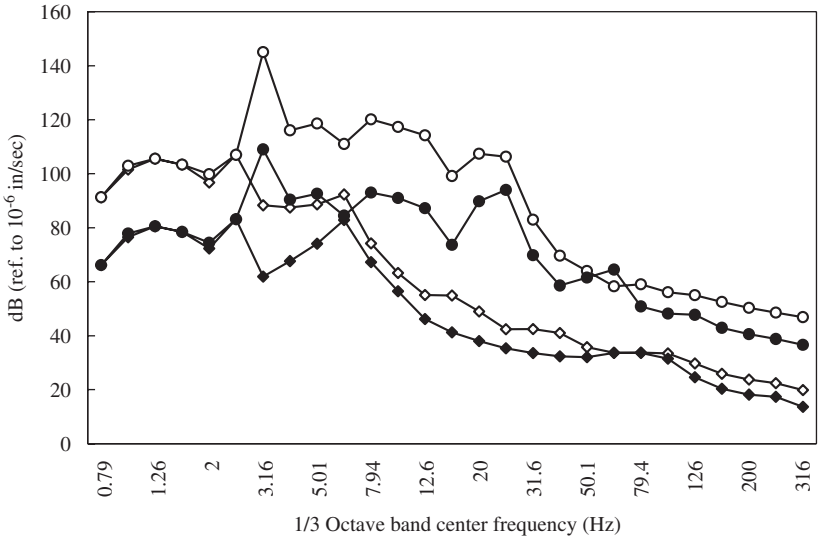

Fig. 16. Vibration spectrum of rail at various slab bearing stiffness (k_b) and train speed (v) combinations, $K_b = 5.8$ kN/mm, $v = 22$ m/s (◇), $K_b = 5.8$kN/mm $v = 80$ m/s (○), $K_b = 5800$ kN/mm, $v = 22$ m/s (♦), $K_b = 5800$ kN/mm, $v = 80$m/s (●) of the dynamic analysis with 0.001 s time increment.

4.3. The effect of slab mass on rail vibration

Increasing foundation mass or slab mass is usually considered as an option of vibration control. The mass of FST may be increased by adding thickness. In this study, slabs with 1640 and 3280 kg/slab were analyzed to reveal if there are any adverse effects on wheel–rail interaction associated with heavyweight slabs. The rail vibrations at various speeds are shown in Fig. 17(a) and wheel–rail contact forces are compared in Fig. 17(b). Rail vibration for the heavyweight slab track is slightly higher in high-speed range. The increase rates of wheel–rail contact force and the maximum vibration level of the heavy slab case are higher than those of normal weight slabs in the speed range of 45–75 m/s. Further analyses are needed to avoid adverse effects for specific combinations of slab thickness and vehicle speed.

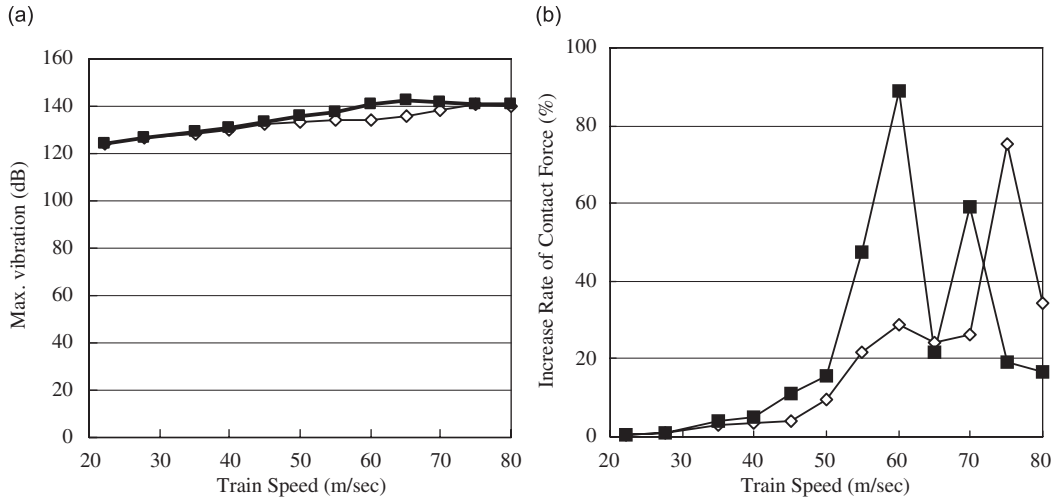

Fig. 17. Various slab mass, 1640 kg (◇), 3280 kg (■) influence (a) maximum vibration level of rail and (b) increase rate of wheel–rail contact force at various train speed.

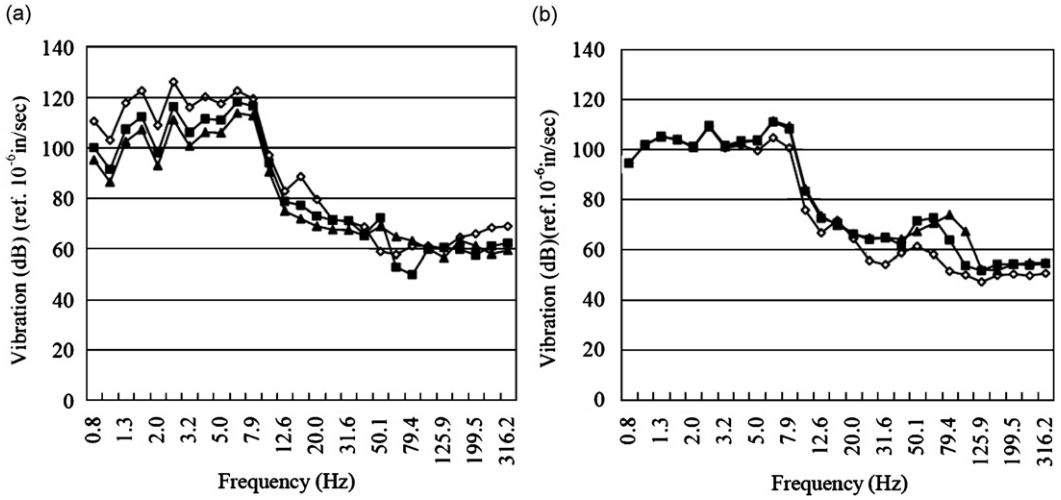

Fig. 18. Effects of various rail clip stiffness, 13kN/mm (◇), 64kN/mm (■), 182kN/mm (▲) on (a) rail vibration and (b) slab vibration.

4.4. The effects of track parameters on slab vibration

The characteristics of slab vibration of FST were examined. Fig. 18(a) shows that soft rail clip induces relatively high level of rail vibration in low-frequency range, but results in low levels of slab vibration in wide frequency range as shown in Fig. 18(a).

Rail vibration levels were found almost unaffected by slab bearing stiffness, as shown in Fig. 19(a). In the other hand, Fig. 19(b) illustrates that the slabs on soft slab bearings vibrate significantly severer than on stiff slab bearing. This phenomenon again justifies that aforementioned conclusion that soft supports are likely to ease vibrations beneath them, but may enlarging vibrations between the supports and loading sources. In other words, soft rail clip may reduce slab vibrations, but increase rail vibration which affects riding comfort. To reduce vibration transmitting to bridge deck or subgrade, soft slab bearing might be effective. Yet, the slabs resting on the bearings may vibrate more.

Normally, it is desirable to lower wheel–rail force and track deflection to ensure riding quality and train stability and to reduce force transmission to subgrade for environmental concerns. The goal could be achieved

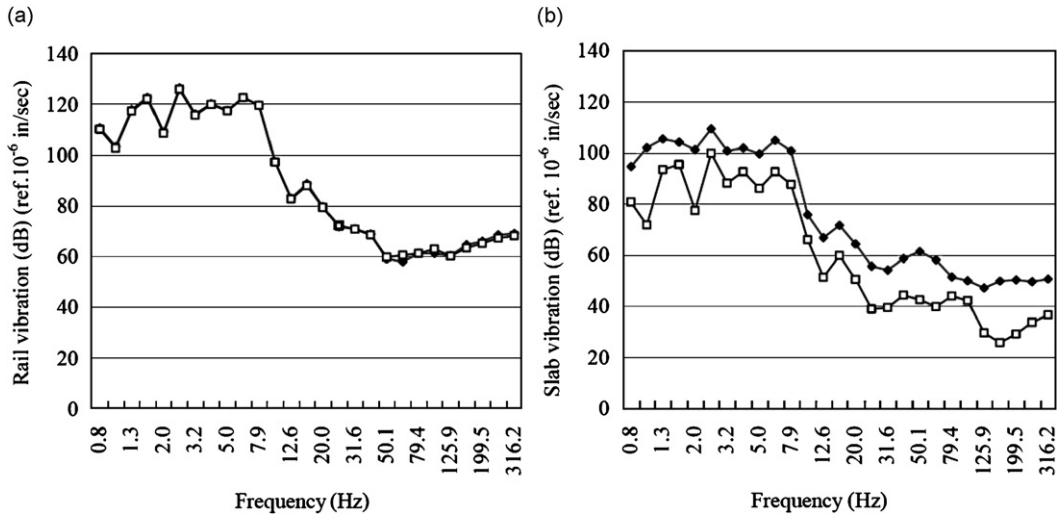

Fig. 19. Effects of various slab bearing stiffness, 5.8 kN/mm (◆), 180kN/mm (□) on (a) rail vibration and (b) slab vibration.

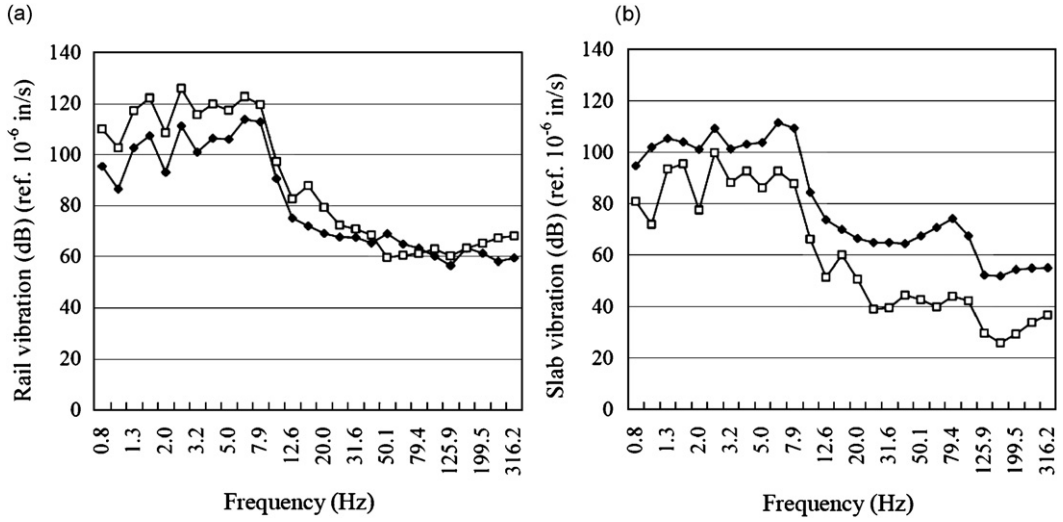

Fig. 20. Comparison of (a) rail vibration spectrum and (b) slab vibration spectrum of two combinations of rail clip stiffness (K_p) and slab bearing stiffness (K_b), $K_p = 182$ kN/mm, $K_b = 5.8$ kN/mm (◆), $K_p = 13$ kN/mm $k_b = 180$ kN/mm (□).

with the combination of stiff rail clip and soft slab bearing. The rail vibration is lower than the case with soft rail clip as shown in Fig. 20(a). However, Fig. 20(b) also illustrate that vibrations might be trapped in the layer of floating slabs for the case of stiff rail clip and soft slab bearing. This result agrees with the conclusion by Hussein and Hunt [29] stating that soft slab-bearings is important in decreasing the vibration levels by confining the energy in the slab. Influences of this phenomenon and resolving means will be addressed in the upcoming study.

5. Conclusions

A coupled system of FST and wheels with suspended mass were derived and solved with Runge–Kutta method. The model was satisfactorily validated along with convergence study. Vibration level and contact forces on rail of various combinations of track parameters were compared to explore the effects of FST on

track itself. The design parameters considered in this study include stiffness of rail clip, stiffness of slab bearing, and slab mass. The results are summarized as follows:

1. For a specific traveling speed, tracks with stiff rail clips undergo higher deflections and wheel–rail contact forces than tracks with soft rail clips. As for slab bearings, low stiffness designs reduce outspreading vibrations, but enlarge deflections and vibrations between the bearings and the loading.
2. Stiffness of slab bearing and slab mass are effective in altering rail vibration levels at frequencies above 20 Hz. The reduction magnitude depends on track irregularities. For smooth running top, redistribution of supporting reactions might be more critical than vibration mitigation.
3. Arbitrary designs of FST may cause amplification of dynamic responses in rail and slabs at medium–high speeds. Proper design and analysis are needed to ensure riding quality and track life.
4. The combination of stiff rail clip and soft slab bearing can take care of environmental vibration problems and excess rail responses. The energy trapped in the layer of slabs should be resolved to make this design concept feasible in practice.

Acknowledgment

This work was supported in part by the National Science Council under the Grant NSC93-2218-E-006-021.

References

[1] G.P. Wilson, H.J. Saurenman, J.T. Nelson, Control of ground-borne noise and vibration, *Journal of Sound and Vibration* 87 (2) (1983) 339–350.
[2] Hussein Mohammed, Dynamic effect of slab discontinuity on underground moving trains, *Proceedings of the Eleventh International Congress on Sound and Vibration*, St. Petersburg, Russia, 2004.
[3] J.P. Talbot, 2000. Reduction of train-induced vibration in buildings, in: *Engineering Transactions*, Vol. 48 (3), Polish Academy of Sciences, Institute of Fundamental Technological Research.
[4] C.J.C. Jones, Use of numerical models to determine the effectiveness of anti-vibration systems for railways, *Proceedings of the Institution of Civil Engineers-Transport* 105 (1994) 43–51.
[5] J.T. Nelson, Recent developments in ground-borne noise and vibration control, *Journal of Sound and Vibration* 193 (1) (1996) 367–376.
[6] Esveld. Coenraad, *Modern Railway Track*, second ed, MRT-Production, The Netherland, 2001.
[7] Jong-Shyong. Wu, Po-Yun. Shih, The dynamic behaviour of a finite railway under the high-speed multiple moving forces by using finite element method, *Communications in Numerical Methods in Engineering* 16 (2000) 851–866.
[8] M. Hetenyi, *Beams on Elastic Foundation*, University of Michigan Press, Ann Arbor, MI, 1946.
[9] L. Frÿba, *Vibrations of solids and structures under moving loads*, Noordhoff International Publishing, Groningen, The Netherlands, 1972.
[10] K.L. Knothe, S.L. Grassie, Modelling of railway track and vehicle/track interaction at high frequencies, *Vehicle System Dynamics* 22 (1993) 209–262.
[11] J.A. Forrest, Experimental modal analysis of three small-scale vibration isolator models, *Journal of Sound and Vibration* 289 (1–2) (2006) 382–412.
[12] F. Cui, C.H. Chew, The effectiveness of floating slab track system—Part. Receptance methods, *Applied Acoustics* 61 (2000) 441–453.
[13] A.R. Crockett, J.R. Pyke, Viaduct design for minimization of direct and structure-radiated train noise, *Journal of Sound and Vibration* 231 (2000) 883–897.
[14] M.F.M. Hussein, H.E.M. Hunt, 2003. An insertion loss model for evaluating the performance of floating-slab track for underground railway tunnels, *10th International Congress on Sound and Vibration*, ICSV1, Stockholm, Sweden.
[15] M.F.M. Hussein, H.E.M. Hunt, Modelling of floating-slab tracks with continuous slabs under oscillating moving loads, *Journal of Sound and Vibration* 297 (1–2) (2006) 37–54.
[16] G. Lombaert, et al., The control of ground-borne vibrations from railway traffic by means of continuous floating slabs, *Journal of Sound and Vibration* 297 (3–5) (2006) 946–961.
[17] J.A. Forrest, H.E.M. Hunt, A three-dimensional tunnel model for calculation of train-induced ground vibration, *Journal of Sound and Vibration* 294 (4–5) (2006) 678–705.
[18] T. Balendra, K.H. Chua, K.W. Lo, S.L. Lee, Steady-state vibration of subway-soil-building system, *Journal of Engineering Mechanics, ASCE* 115 (1) (1989) 145–162.
[19] Piers Connor, Modern Railway Glossary, Railway Technical Web Pages, 〈http://www.trainweb.org/railwaytechnical/newglos.html〉, 2004.

[20] C.-W. Tseng, Dynamic Analysis of Railway Track with Three-dimension Finite Element Method, M.S. Thesis, National Cheng Kung University, Taiwan, 2001 [in Chinese].
[21] K. Knothe, S.L. Grassie, J.A. Elkins, *Interaction of Railway Vehicles with the Track and its Substructure*, Swets & Zeitlinger B.V., 1995.
[22] W. Zhai, *Vehicle–Track Coupling Dynamics*, China Railway Press, Beijing, 2002.
[23] D. Young, Vibration of rectangular plates by the Ritz method, *Journal of Applied Mechanics* 17 (1950) 448–453.
[24] Y.B. Yang, J.D. Yau, *Theory of Vehicle–Bridge Interaction for High Speed Railway*, DNE Publisher, Taiwan, 2000 [in Chinese].
[25] W.T. Thomson, *Theory of Vibration with Applications*, second ed., Prentice-Hall, Englewood Cliffs, NJ, 1981.
[26] R.I. Mair, The influence of rail flexibility between supports on track natural frequency, *Railway Track & Structures* 1980 (July) (1980) 29–30.
[27] H. Takemiya, Simulation of track–ground vibrations due to a high-speed train: the case of X-2000 at Ledsgard, *Journal of Sound and Vibration* 261 (3) (2003) 503–526.
[28] D.S. Hsu, K.C. Tseng, S.H. Yeh, Strategies of reducing vibration with trench in southern Taiwan Science Park, *Conference of Vibration Reduction in Southern Taiwan Science Park*, November 27, 2001, pp. 61–89 [in Chinese].
[29] M.F.M. Hussein, H.E.M. Hunt, An insertion loss model for evaluating the performance of floating-slab track for underground railway tunnels, *10th International Congress on Sound and Vibration, ICSV10*, Stockholm, Sweden, 2003.